Applied Physics A (2022) 128:574
https://doi.org/10.1007/s00339-022-05721-8

Applied Physics A
Materials Science & Processing

Assessment of $Fe_xSe_{0.5}Te_{0.5}$ alloy properties for ionizing radiation shielding applications: an experimental study

R. M. Hamad[1] · M. Kh. Hamad[2] · N. Dwaikat[1,3] · Kh. A. Ziq[1,3]

Received: 30 March 2022 / Accepted: 22 May 2022 / Published online: 11 June 2022
© The Author(s), under exclusive licence to Springer-Verlag GmbH, DE part of Springer Nature 2022

Abstract
We investigate the radiation shielding properties of $Fe_xSe_{0.5}Te_{0.5}$ ($0.95 \le x \le 1.05$) polycrystalline samples prepared by a conventional solid state reaction method. The mass attenuation coefficient (MAC) was measured experimentally, and the obtained results are then benchmarked with the simulated data from XCOM (Photon cross sections database). The experimental results exhibit a reasonable correlation with the XCOM data with relative difference between 0.4 and 4.1%. The Kolmogorov–Smirnov (K–S) test further ascertained from a statistical point of view that the experimentally measured data matched very well the data obtained from the XCOM with the maximum vertical deviation (D_n) between 0.33% and 1.17% in all samples. Based on the MAC, different radiation shielding parameters such as linear attenuation coefficient (LAC), half-value layer (HVL), mean free path (MFP), transmission factor (TF), and radiation protection efficiency (RPE) were determined for all investigated alloys. The results indicate that the $Fe_{0.95}Se_{0.5}Te_{0.5}$ ($x = 0.95$) sample has superior shielding features compared to other iron content samples. These findings suggest that this alloy can be used in the ionizing radiation shielding applications.

Keywords Fe-based polycrystalline alloys · Radiation shielding properties · XCOM software

1 Introduction

Alloys of metals and other elements such as metals, nonmetals, or metalloids enhances various physical properties of metals [1]. During alloys studying, several factors must be considered as its grain size, solubility, composition, melting temperatures and preparation technique [2]. Many factors can affect crystalline structure and physical properties, such as the solidification processes; nucleation of crystals or crystals growth, substitution or doping during the preparation [3]. Controlling the flow of stresses in the solid phase is one of the most important difficulties during solidification processes. The collapse of temperature of molten material permits freezing which causes a dropping of the solubility of the alloying elements. The addition of some elements to the prepared alloys may significantly modify some of its physical properties [4, 5]. For example, the addition of Boron and Carbon to Titanium alloys improved their strengths and heat resistance [6]. Lithium when added to aluminum alloys decreases the heat conductivity and increases the elasticity [7]. Antimony substituted $CrTe_{1-x}Sb_x$ ($0 \le x \le 0.2$) alloys increases entropy change and affecting the magnetic state of the alloy [8]. Adding of Molybdenum and Vanadium to Fe_3AL alloys improved their mechanical properties as strength, ductility, and bulk hardness [9].

Ionizing Radiations are widely used in medical, agricultural, geological, and fundamental scientific studies. Safety is the main challenge facing the facility users. The potential adverse effects of ionizing radiation were realized early on, a few years after W. Roentgen discovered the x-rays. Occupants need to keep up with the ALARA principle; in particular, the three major factors in radiation protection: exposure

✉ M. Kh. Hamad
morad.hamad@htu.edu.jo

✉ N. Dwaikat
ndwaikat@kfupm.edu.sa

[1] Physics Department, College of Engineering and Physics, King Fahd University of Petroleum and Minerals, Dhahran 31261, Saudi Arabia

[2] Department of Basic Sciences, School of Social and Basics Sciences, Al Hussein Technical University, King Abdullah II St 242, Amman 11831, Jordan

[3] Interdisciplinary Research Center for Advanced Materials, King Fahd University of Petroleum and Minerals, Dhahran 31261, Saudi Arabia

time, distance, and shielding. The selection of shield material depends on the type and energy of radiation while the amount of radiation reduction depends on the thickness and density of the shielding material [1]. These features render the materials to be the most sought factor for radiation shielding purposes in medical uses and industrial applications. Recently, new groups of radiation shielding materials were used in radiation protection environment; these include but not limited to alloys [1], glasses [10], ceramics [11, 12], polymers [13], and multi layered composite materials [14, 15]. The use of the metallic alloys as an alternative protective shielding material has attracted a lot of attention due to several short coming of the conventional shielding materials.

Many parameters can be determined from the mass attenuation coefficient (MAC), as the mass energy absorption, total interaction cross-section, the effective atomic number (Z_{eff}) and effective electron density (N_{eff}). Several theoretical and experimental studies were devoted to calculating these parameters. Limkitjaroenporn et al. measured mass attenuation coefficients (MAC) and effective atomic numbers (Z_{eff}) for Inconel 738 super-alloy for different energies obtained from Compton scattering in range between 223 and 662 keV [16]. Inconel 738 super-alloy is considered one of the best materials for the radiation shielding; it consists of 61.5% of Ni and 16 other elements. Han and Demir studied mass attenuation coefficients (MAC), effective atomic numbers (Z_{eff}) and effective electron density (N_{eff}) for Cr, Fe, Ni and Au alloys at different photon energies [17, 18]. Mohammed et al. investigated mass attenuation coefficients (MAC) for $Ni_{100-x}Al_x$, $Zn_{100-x}Al_x$ and mixtures with different weight ratios using Am-241 at 0.04 Ci [19]. Transmission experiments in the photon energy region 60–400 keV for W/Cu alloy of two compositions 65/35 and 60/40 were conducted and the photon cross sections were evaluated by Murthy et al. [20, 21]. Total attenuation cross sections in four alloys: telphy, dilver P, anhyster DS, and anhyster M, at 32.1, 52, 72.1, 84.3, 145.4, 279.2, and 661.6-keV photon energies were measured by Babu et.al using two NaI(Tl) scintillation detectors [22]. Kaur et al. prepared five alloys of Pb and Sn in different compositions and explored different shielding parameters: mean free path (MFP), effective atomic number (Z_{eff}), and effective electron density (N_{eff}) in the wide energy ranges from 1.0 keV to 100.0 GeV [23]. Krishna et al. pointed out [24] that the total photon cross sections in five Nickle-based alloys, viz., Superimphy, Inconel, Nimonic-90, Invar, and stainless steel at photon energies of 32.1, 52.0, 72.1, 84.3, 145.4, 279.2, 320.0, and 661.6 keV are in good agreement with theoretical values.

Iron-based alloys are expected to have good properties in radiation shielding because of the high density, high strength, and corrosion resistance. Blink et al. [25] proposed a Fe-based alloy with 14 wt% Boron for neutrons absorption for nuclear waste storage uses. The shielding parameters: (HVL), (MFP), (N_{eff}), and (Z_{eff}) of steel alloys were measured by Al-Jaff [26] and he determined the relation between these parameters with photon energy and electron density. A comprehensive study of photon interaction with alloys containing iron and steel slag were conducted and shielding parameters were calculated at various photon energies by Singh et al. [27].

Recently, we investigated the radiation shielding properties of five iron-based ($Fe_xSe_{0.5}Te_{0.5}$) single crystals using SRIM code and Phy-X program [2]. The results revealed that the single crystals with iron content ($x = 0.95$) has a good radiation shielding properties compared with other iron contents. These FeSe alloy have been found by Hosono et al. [28] to be superconductors with transition temperature ~ 9 K. Moreover, the Fe-based alloys consist of layers of iron and an element from group 15 in the periodic table, like Arsenic and Phosphorus. Several properties of these alloys ($FeSe_{0.5}Te_{0.5}$) have been extensively studied; crystal structure, critical temperature T_c ~ 15 K [29]. However, to the best of our knowledge, there is no reported radiation shielding properties for this polycrystalline alloy.

In this article, we aimed to develop environmentally friendly shielding radiation material that is effective over a wide range of energies. It is a continuation of our earlier work on single crystals [2, 29]. Furthermore, to investigate effect of iron content in radiation shielding parameters, such as the mass attenuation coefficient (MAC), linear attenuation coefficient (LAC), half-value layer (HVL), mean free path (MFP), and the projected range for different $Fe_xSe_{0.5}Te_{0.5}$ polycrystalline alloys at the photon energy values 0.184, 0.28, 0.662, 0.71 and 0.81 MeV. The mass attenuation coefficient (MAC) values of the investigated alloys have been computed theoretically using XCOM software to test the confirmation of the experimental results.

2 Materials and methods

High purity (99.99% or higher) Fe, Se and Te elements were used to prepare $Fe_xSe_{0.5}Te_{0.5}$ polycrystalline samples. Stoichiometric ratios of the elements were used to prepare five samples with ($0.95 \le x \le 1.05$) according to Table 1. The

Table 1 Composition ratio for all alloy samples

Sample	Code	Molecular weight (g/mol)	Density (g/cm^3)
$Fe_{0.95}Se_{0.5}Te_{0.5}$	FST95	156.338	5.7971
$Fe_{0.98}Se_{0.5}Te_{0.5}$	FST98	158.014	5.3892
$FeSe_{0.5}Te_{0.5}$	FST100	159.131	5.1450
$Fe_{1.02}Se_{0.5}Te_{0.5}$	FST102	160.247	4.8211
$Fe_{1.05}Se_{0.5}Te_{0.5}$	FST105	161.923	4.4603

powdered elements were mixed and grind using an agate mortar for about 20 min then pressed into pellets. The pellets were encapsulated in a quartz tube and sealed at partial pressure of high purity Argon gas. All samples were initially annealed at 300 °C and 500 °C for 5 h at each temperature, and then heated to 800 °C and held for 10 h. After that, the temperature was gradually reduced to 400 °C in about 120 h then cooled to room temperature. The samples were re-grinded thoroughly, pressed in pellets then sealed in quartz tube under partial Argon pressure and re-annealed at 400 °C for 50 h and furnace cooled to room temperature.

The density for each alloy was measured using a sensitive density balance (~ 10^{-4} g) and Archimedes principle with distilled water as an immersion fluid. The measured densities were used in calculating the linear attenuation coefficient (LAC).

For the radiation shielding properties, a narrow gamma-beam setup was built in the nuclear physics lab at the King Fahd University of Petroleum and Minerals (KFUPM). The setup consists of two radioactive sources (^{137}Cs with 0.662 MeV, and ^{166}Ho with 0.184, 0.280, 0.71, and 0.810 MeV), three steps collimator, and a detection system. The detailed experimental setup and measurement methods are described elsewhere [30].

3 Results and discussions

Room temperature X-ray diffraction (XRD) of the prepared alloys have been investigated and published elsewhere [29]. The results of refinement revealed a PbO-tetragonal structure which can be described using the P4/nmm space group symmetry with some minor impurity phases (< 10%). The impurity phases were found to diminish with increasing Fe content. The mass attenuation coefficient (MAC) of the $Fe_xSe_{0.5}Te_{0.5}$ polycrystalline alloys was measured experimentally at the mentioned-above selected energies. The results are then benchmarked with the XCOM results (see Table 2). The relative difference (RD%) between experimental and theoretical measurements is calculated according to:

$$\mathrm{RD}\% = \frac{(\frac{\mu}{\rho_{\mathrm{Th}}}) - (\frac{\mu}{\rho_{\mathrm{Exp}}})}{(\frac{\mu}{\rho_{\mathrm{Th}}})} \times 100\%.$$

To assess how well the experimental data represents the obtained data from XCOM from a statistical point of view, a Kolmogorov–Smirnov (K-S) test for all investigated alloys. The test covers the range of all available incident energies (0.184–0.810 MeV). The K-S test is based on evaluating the Cumulative Distribution Fraction (CDF) function of the two data sets (i.e. experimental and simulated data) and calculate the maximum vertical deviation (D_n) between both functions. A small deviation (D_n) implies that the measured data (experimental) match the XCOM data (simulated) very well [31, 32]. In other words, if the two CDF of the data set are not very different, then they are very well matched. Figure 1 shows the CDF functions for both measured and simulated MAC of $Fe_{0.95}Se_{0.5}Te_{0.5}$ sample. Both CDF functions in Fig. 1 harmonize completely. In addition, the K-S test gives $D_n = 0.0096$ with a corresponding p value that is equal to 0.983 which is close to one, implies that the two data set are mutually consistent. Similar analyses were applied to the rest of samples and the results are shown in Fig. 2.

The linear attenuation coefficient (LAC) for all prepared samples have been measured using selected gamma energies

Table 2 The experimental mass attenuation coefficient (MAC) and the RD % for the prepared alloys compared to the XCOM calculated values

Energy (MeV)	Result type	$Fe_{0.95}Se_{0.5}Te_{0.5}$	$Fe_{0.98}Se_{0.5}Te_{0.5}$	$FeSe_{0.5}Te_{0.5}$	$Fe_{1.02}Se_{0.5}Te_{0.5}$	$Fe_{1.05}Se_{0.5}Te_{0.5}$
0.184	XCOM	0.26940	0.26830	0.26750	0.26670	0.26560
	Experimental	0.26591	0.26529	0.25830	0.26152	0.25509
	RD (%)	1.3	1.1	3.4	1.9	3.9
0.280	XCOM	0.14560	0.14520	0.1450	0.14480	0.14450
	Experimental	0.14969	0.14991	0.14439	0.14552	0.14631
	RD (%)	2.8	3.2	0.4	0.5	1.2
0.662	XCOM	0.07295	0.07296	0.07296	0.07297	0.07297
	Experimental	0.07527	0.07153	0.07009	0.071654	0.07468
	RD (%)	3.2	1.9	3.9	1.8	2.3
0.71	XCOM	0.07000	0.07001	0.07002	0.07003	0.07004
	Experimental	0.07154	0.068661	0.06714	0.06821	0.07025
	RD (%)	2.2	1.9	4.1	2.6	0.3
0.81	XCOM	0.06490	0.06492	0.06493	0.06495	0.06496
	Experimental	0.06635	0.06379	0.06203	0.06283	0.06385
	RD (%)	2.2	1.7	4.5	3.3	1.7

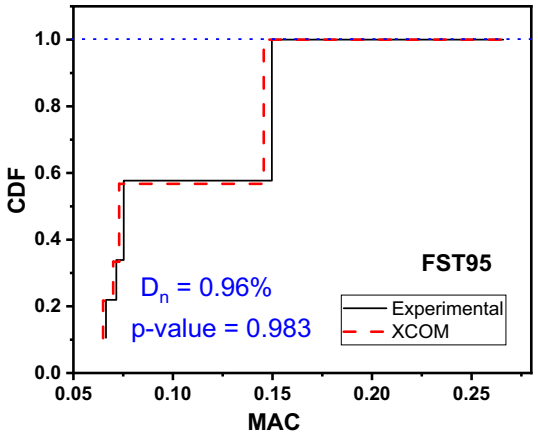

Fig. 1 The cumulative distribution functions CDF of the simulated MAC using XCOM and of the experimental data for FST95 sample. Both CDF functions coincide, and therefore the maximum vertical deviation D_n was found very small (see text)

from ^{137}Cs and ^{166}Ho radiation sources. The LAC is obtained using the lambert law: $I = I_o e^{-\mu x}$, where I, I_o, μ and x are the transmitted and the incident photon beam intensities, the attenuation coefficient, and the sample thickness, respectively. To calculate the MAC, we simply used MAC $= \frac{\mu}{\rho}$, for each sample. Figure 3 shows the variation of the linear attenuation coefficient with energy for all studied alloys. The experimental behavior is then fitted according to the exponential decay equation shown in the figure. The LAC for all studied samples decreases gradually with increasing the energy. This is normal behavior because the density of the samples (the number of atoms per unit volume) decreases with increasing the Fe content and the interaction probability between gamma photons and material decreases as well. The highest LAC (in cm^{-1}) is reported at the lowest photon energy (i.e. $E = 0.184$ MeV) that is equal to 1.562, 1.433, 1.329, 1.286, and 1.138 for FST95, FST98, FST100, FST102, and FST105 respectively. These values are found to be decreasing with increasing the incident photon energy, indicating that the thickness of these alloys needs to be

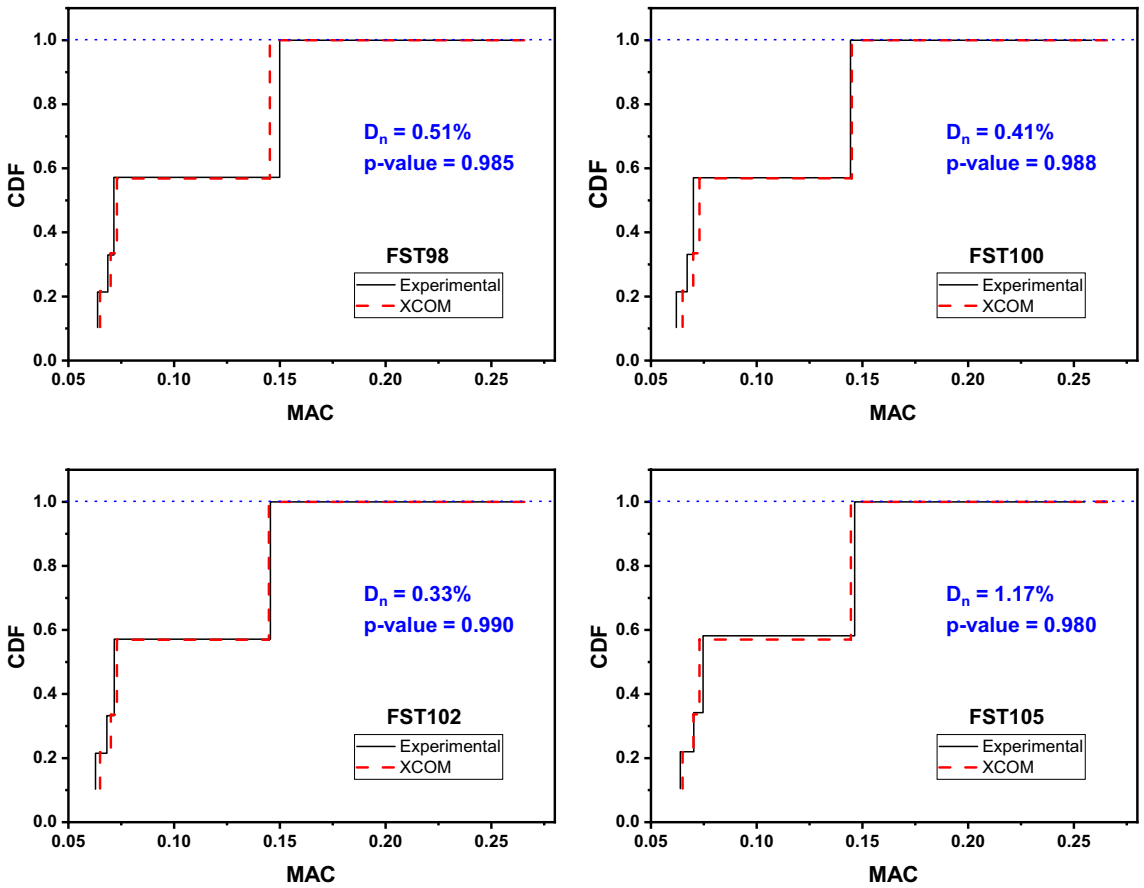

Fig. 2 The cumulative distribution functions CDF of the simulated MAC using XCOM and of the experimental data for FST98, FST100, FST102, and FST105 samples. Both CDF functions coincide for all samples, and therefore the maximum vertical deviation D_n was found very small

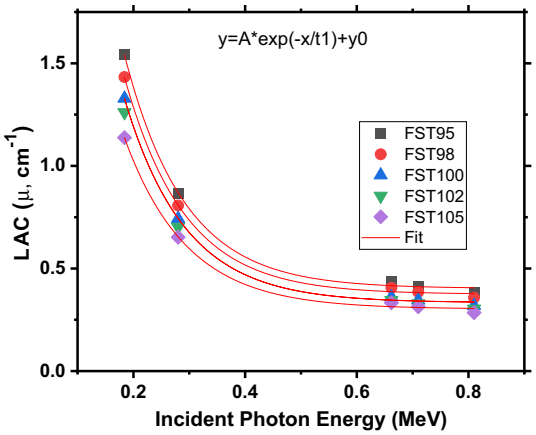

Fig. 3 Variation of the measured Linear attenuation coefficient with energy for $Fe_xSe_{0.5}Te_{0.5}$ (x=0.95, 0.98, 1.00, 1.02, and 1.05) samples

increasing when dealing with relatively higher energies. This behavior can be attributed to the Compton scattering which is dominant interaction between photons and the prepared alloys in the used range of energy in this study [33]. Figure 4a and b shows the variation of the experimental LAC with sample density and Fe content at 0.184 MeV respectively. It is noticed that the linear attenuation coefficient (LAC) increases with increasing the density (number of atoms per unit volume), which results in increasing the interaction probability (cross-section) of photons with the medium. This is consistent with the radiation shielding basic knowledge, which is approved by the results in Fig. 3. This behavior can also be attributed to the Compton scattering in the used energy range where the photons have less ability to penetrate materials with the highest densities (less collisions at high density). These two factors (i.e. photons energy and material density) are greatly affecting the linear attenuation coefficient.

In Fig. 5a we present the experimental half-value layer (HVL) for the investigated $Fe_xSe_{0.5}Te_{0.5}$ samples versus the incident photon energy used in this study. The HVL is obtained using $HVL = \frac{0.693}{\mu}$ inversely proportional to LAC. The figure reveals an increase in the HVL with increasing energy and a decrease with increasing the sample density. The FST95 sample is the most efficient sample in radiation attenuation compared to other samples. The lowest HVL among the five prepared samples is observed at 0.184 MeV and settle within the range of 0.45 cm for the FST95 sample to 0.61 for the FST105 sample. On the contrary, the highest HVL is seen at 1.80, 1.94, 2.17, 2.29, and 2.43 cm for the FST95, FST98, FST100, FST102, FST105 respectively which occurs at 0.81 MeV incident beam energy. It is worth mentioning that the half-value layer shows opposite behavior to the linear attenuation coefficient at the same incident photon energy.

Figure 5b shows a comparison between the HVL of investigated FST95 sample in this study with different materials published in the literature. For instance, when the incident photon energy is equal to 0.81 MeV, the reported HVL for the concrete (BC), RS 360 (RS) glass, SnTe and PbTe alloys are 2.76, 2.32, and 2.09 cm respectively [2, 34], which are much thicker than our best experimental HVL value 1.80 cm for FST95 sample. However, it is thinner than the HVL for the reported PbTe which equals to 1.34 cm (see Fig. 6). Similar behavior has been seen for all used energies.

The mean free path is another important factor in the radiation shielding features it is defined as the distance between two successive collisions. It depends on the density of the interaction medium, and the energy of the incident radiation as shown in Fig. 7. It decreases with the increases in the density of the medium because increases the number of collisions which leads to the incident photons losing their energies within a short distance. Also, it increases with the energy of the radiation because photons with high

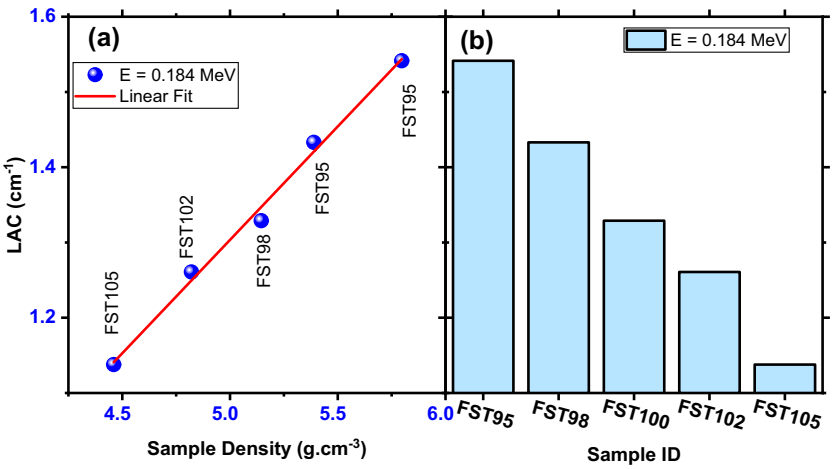

Fig. 4 The variation of LAC with **a** sample density, and **b** the bar-graph of the investigated samples

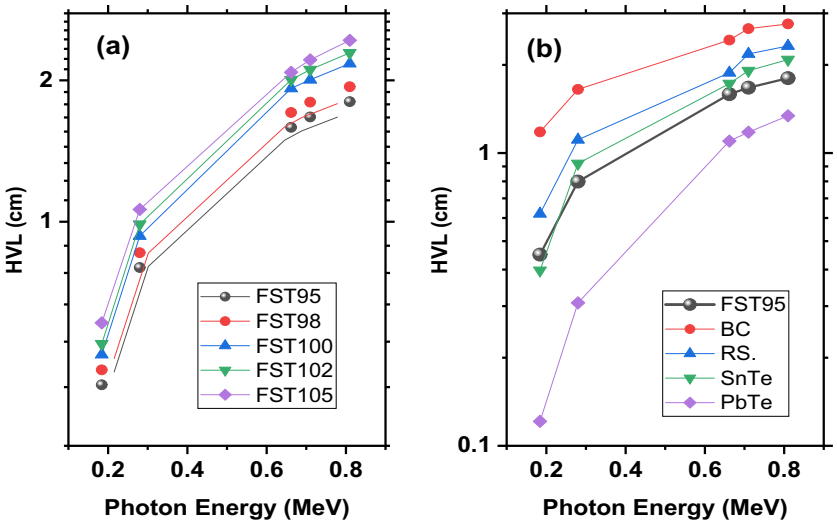

Fig. 5 **A** The experimental Half-value layer (HVL) for the $Fe_xSe_{0.5}Te_{0.5}$ ($x=0.95$, 0.98, 1.00, 1.02, and 1.05) samples. **b** A comparison between the FST95 sample from this study with published HVL for different compounds

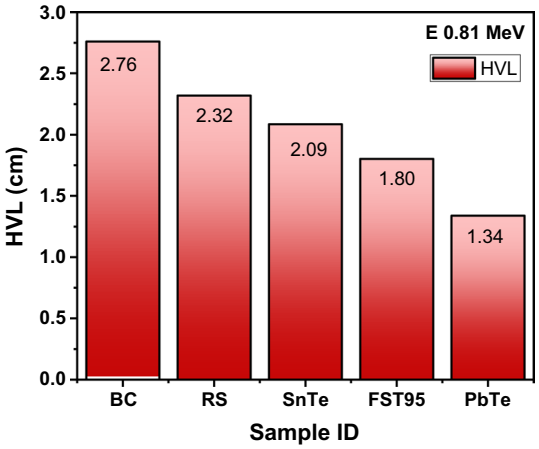

Fig. 6 Comparison between the HVL of the FST95 sample prepared in this study with reported alloys published in the literature

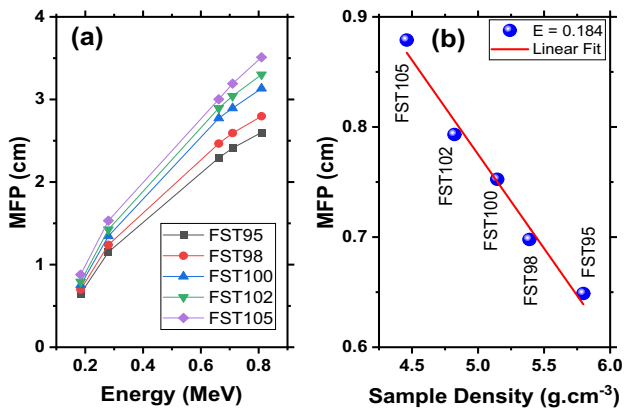

Fig. 7 The mean free path (MFP) for the investigated alloys at **a** different incident energies. **b** Different sample density at constant energy of 0.81 MeV

energy can survive for a long time and do more collisions as shown in Fig. 7. It can be calculated from the LAC, where MFP $= \mu^{-1}$. The MFP of the investigated alloys is shown in Fig. 7a. The results reveal that the MFP is an energy dependent factor. That means any increasing in the incident photon energy leads to increase the MFP value for the investigated samples. Figure 7b shows the MFP for all samples at specific energy ($E=0.81$ MeV). The highest MFP is observed for the FST105 sample which has the lowest density that is equal to 0.879 cm while on the other hand the lowest MFP is 0.649 cm which is for the FST95 sample with the highest density.

To evaluate the impact of the prepared alloys on the radiative attenuation properties, we obtained the transmission factor (TF). This factor describes the number of gamma rays that penetrates through the shielding material. A smaller TF value indicates better shielding properties. Moreover, the radiation protection efficiency (RPE) is also employed to evaluate the efficiency of the prepared alloys as shielding materials in absorbing the incident photon beams. Both, TF and RPE are obtained according to $\mathrm{TF} = \frac{I}{I_o} \times 100\% = e^{-\mu x} \times 100\%$ and $\mathrm{RPE} = (1 - e^{-\mu x}) \times 100\%$ respectively. Figure 8a shows the TF (in log scale) for the prepared alloys at energy of 0.662 MeV versus the sample thickness in cm (linear scale), and the results are fitted linearly. the comparison of TF for all alloys is clearly seen from the figure. For example, when the sample thickness is 5 cm, the TF for the FST95 is about 11% while it is about 18% for the FST105. This difference reaffirms the better shielding ability for the FST95 sample among the rest of samples. Figure 8b shows the RPE (in log scale) for the samples at 0.662 MeV versus the sample thickness (linear scale). The RPE shows the samples' ability to attenuate the radiation effectively,

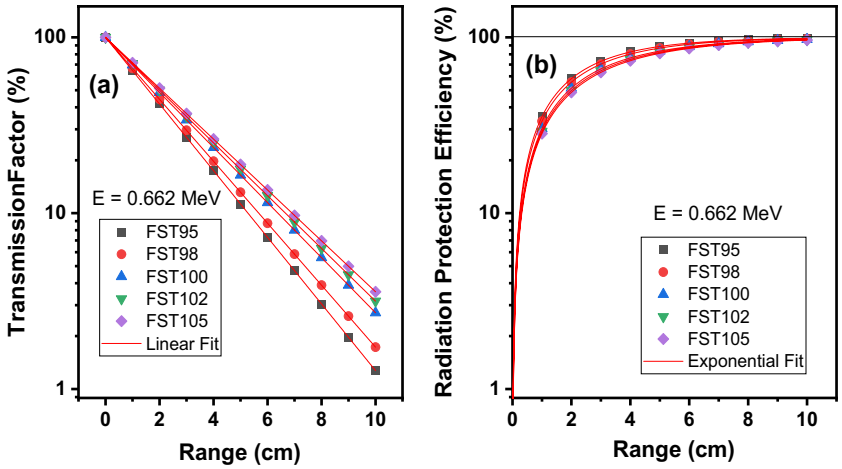

Fig. 8 **a** The transmission factor of the prepared samples versus the thickness for each sample at $E = 0.662$ MeV. **b** The Radiation protection efficiency versus the thickness for the prepared samples versus the thickness at $E = 0.662$ MeV

where it increases exponentially with sample thickness until it reaches the saturation (100%) when the sample has a sufficient thickness. For example, the analysis shows that the RPE at 5 cm is about 89%, 87%, 84%, 82%, and 81% for FST95, FST98, FST100, FST102, and FST105 respectively. This means that these samples can reduce about 80% of the 0.662 MeV incident beam if the sample thickness is 5 cm.

4 Conclusion

The effect of different Fe content on the gamma radiation shielding properties of the $Fe_xSe_{0.5}Te_{0.5}$ polycrystalline alloys was studied at 0.662, 0.184, 0.280, 0.710, and 0.810 MeV gamma energies. The experimental results are, within the accepted uncertainty level, in good agreement with the theoretical values calculated by the X-COM code. Increasing the Fe content affected the most important radiation shielding parameter, linear attenuation coefficient (LAC), and the parameters that are derived from it such as HVL, MFP, transmission factor, and range. The linear attenuation coefficient decreases with increasing the Fe content because the density of samples decreases with the increasing Fe content. The best values for all shielding parameters were achieved at 0.95 Fe content level, which confirmed that $Fe_{0.95}Se_{0.5}Te_{0.5}$ has the most potential for radiation shielding applications. The $Fe_xSe_{0.5}Te_{0.5}$ polycrystalline alloys have a low HVL compared with many materials such as BC, RS glass, and some alloys (SnTe).

Acknowledgements The authors would like to acknowledge the support provided by King Abdulaziz City for Science and Technology (KACST) through the Science and Technology Unit at King Fahd University of Petroleum and Minerals (KFUPM) for funding this work through project No. 11-ADV1631-04 as part of the National Science, Technology and Innovation Plan.

Data availability The datasets generated during and/or analyzed during the current study are available from the corresponding author on reasonable request.

References

1. T. Kaur, J. Sharma, T. Singh, Review on scope of metallic alloys in gamma rays shield designing. Prog. Nucl. Energy. **113**, 95–113 (2019). https://doi.org/10.1016/j.pnucene.2019.01.016
2. R.M. Hamad, M.H.A. Mhareb, Y.S. Alajerami, M.I. Sayyed, G. Saleh, M.K. Hamad, K.A. Ziq, A comprehensive ionizing radiation shielding study of $Fe_xSe_{0.5}Te_{0.5}$ alloys with various iron concentrations. J. Alloys Compd. **858**, 157636 (2021). https://doi.org/10.1016/j.jallcom.2020.157636
3. P. Li, V.I. Nikitin, E.G. Kandalova, K.V. Nikitin, Effect of melt overheating, cooling and solidification rates on Al–16wt%Si alloy structure. Mater. Sci. Eng. A **332**, 371–374 (2002). https://doi.org/10.1016/S0921-5093(01)01864-0
4. U. Kumar Mohanty and H. Sarangi, Casting Processes and Modelling of Metallic Materials- chapter 2: Solidification of Metals and Alloys. BoD–Books on Demand, (2021). https://doi.org/10.5772/intechopen.94393.
5. M. Sherif El-Eskandarany, Mechanical Alloying (Second Edition)- Introduction, William Andrew Publishing, (2015). https://doi.org/10.1016/B978-1-4557-7752-5.00001-2.
6. R. Banoth, R. Sarkar, A. Bhattacharjee, T.K. Nandy, G.V.S. Rao, Effect of boron and carbon addition on microstructure and mechanical properties of metastable beta titanium alloys. Mater. Des. **67**, 50–63 (2015). https://doi.org/10.1016/j.matdes.2014.11.004
7. I. Shiganov, S. Shakhov, L. Tarasenko, A. Plokhikh, Examination of the effect of the speed of laser welding on the structure and properties of aluminium alloys alloyed with lithium and scandium. Weld. Int. **19**, 982–986 (2005). https://doi.org/10.1533/wint.2005.3558
8. M.K. Hamad, E. Martinez-Teran, Y. Maswadeh, R. Hamad, E.G. Al-Nahari, A.A. El-Gendy, K.A. Ziq, Room temperature magnetocaloric effect in $CrTe_{1-x}Sb_x$ alloys. J. Magn. Magn. Mater. **514**, 167171 (2020). https://doi.org/10.1016/j.jmmm.2020.167171
9. R. Baligidad, A. Radhakrishna, A. Datta, V. Rama Rao, Effect of molybdenum addition on structure and properties of high carbon Fe_3Al based intermetallic alloy. Mater. Sci. Eng. A. **313**, 117–122 (2001). https://doi.org/10.1016/S0921-5093(01)00962-5

10. M.H.A. Mhareb, M.I. Sayyed, Y.S.M. Alajerami, M. Alqahtani, N. Dwaikat, A.M. Alsagry, M. Al-Yatimi, M. Zakariah, Structural and radiation shielding features for a new series of borate glass samples: part I. Eur. Phys. J. Plus. (2021). https://doi.org/10.1140/epjp/s13360-020-00984-7
11. D.I. Shlimas, M.V. Zdorovets, A.L. Kozlovskiy, Synthesis and resistance to helium swelling of Li_2TiO_3 ceramics. J. Mater. Sci. Mater. Electron. **31**, 12903–12912 (2020). https://doi.org/10.1007/s10854-020-03843-4
12. M.K. Hamad, M.H.A. Mhareb, Y.S. Alajerami, M.I. Sayyed, G. Saleh, Y. Maswadeh, K.A. Ziq, Radiation shielding properties of $Nd_{0.6}Sr_{0.4}Mn_{1-y}Ni_yO_3$ substitute with different concentrations of nickle. Radiat. Phys. Chem. (2020). https://doi.org/10.1016/j.radphyschem.2020.108920
13. A.H. Abdalsalam, E. Şakar, K.M. Kaky, M.H.A. Mhareb, B. Cevïz Şakar, M.I. Sayyed, A. Gürol, Investigation of gamma ray attenuation features of bismuth oxide nano powder reinforced high-density polyethylene matrix composites. Eur. Phys. J. Plus. **168**, 108537 (2020). https://doi.org/10.1016/j.radphyschem.2019.108537
14. D.I. Tishkevich, S.S. Grabchikov, S.B. Lastovskii, S.V. Trukhanov, T.I. Zubar, D.S. Vasin, A.V. Trukhanov, A.L. Kozlovskiy, M.M. Zdorovets, Effect of the synthesis conditions and microstructure for highly effective electron shields production based on bi coatings. ACS Appl. Energy Mater. **1**, 1695–1702 (2018). https://doi.org/10.1021/acsaem.8b00179
15. D.I. Tishkevich, S.S. Grabchikov, S.B. Lastovskii, S.V. Trukhanov, D.S. Vasin, T.I. Zubar, A.L. Kozlovskiy, M.V. Zdorovets, V.A. Sivakov, A.V. Muradyan, T.R. Trukhanov, Function composites materials for shielding applications: correlation between phase separation and attenuation properties. J. Alloys Compd. **771**, 238–245 (2019). https://doi.org/10.1016/j.jallcom.2018.08.209
16. P. Limkitjaroenporn, J. Kaewkhao, S. Asavavisithchai, Determination of mass attenuation coefficients and effective atomic numbers for Inconel 738 alloy for different energies obtained from Compton scattering. Ann. Nucl. Energy. **53**, 64–68 (2013). https://doi.org/10.1016/j.anucene.2012.08.020
17. I. Han, L. Demir, Determination of mass attenuation coefficients, effective atomic and electron numbers for Cr, Fe and Ni alloys at different energies. Nuclear Instrum. Methods Phys. Res. Sect. B **267**, 3–8 (2009). https://doi.org/10.1016/j.nimb.2008.10.004
18. I. Han, L. Demir, M. Sahin, Studies on effective atomic numbers, electron densities and mass attenuation coefficients in Au alloys. Radiat. Phys. Chem. **18**(1), 39–46 (2010). https://doi.org/10.3233/XST-2010-0238
19. F. Mohammed, R. Razooqi, M. Majeed, , Y.Vijay, S. Surve, Self mass attenuation coefficients for mixture of some 3d elements Ni_{100-x} Al_x and Zn_{100-x}–Al_x at Am-241(40mCi), Int. J. Recent Res. Rev. **3** (2012) 26–31. http://www.ijrrr.com/papers3/paper4.pdf.
20. V.R.K. Murty, D.P. Winkoun, K.R.S. Devan, Effective atomic numbers for W/Cu alloy using transmission experiments. Appl. Radiat. Isot. **53**, 945–948 (2000). https://doi.org/10.1016/S0969-8043(00)00248-7
21. V.R.K. Murty, Effective atomic numbers for W/Cu alloy for total photon attenuation. Radiat. Phys. Chem. **71**, 667–669 (2004). https://doi.org/10.1016/j.radphyschem.2004.04.046
22. K.S. Babu, S.C. Lingam, D.V. Krishna Reddy, Gamma-ray cross sections and effective atomic numbers in some alloys in the energy range 32–662 keV. Can. J. Phys. **62**, 5 (1984). https://doi.org/10.1139/p84-028
23. S. Kaur, A. Kaur, P.S. Singh, T. Singh, Scope of Pb-Sn binary alloys as gamma rays shielding material. Prog. Nucl. Energy. **93**, 277–286 (2016). https://doi.org/10.1016/j.pnucene.2016.08.022
24. D.V. Krishna Reddy, K.S. Babu, S.C. Lingam, Photon cross sections and effective atomic numbers in some alloys. Can. J. Phys. (1985). https://doi.org/10.1139/p85-237
25. J. Blink, J. Farmer, J. Choi, C. Saw, Applications in the nuclear industry for thermal spray amorphous metal and ceramic coatings. Metall Mater. Trans. A Phys. Metall. Mater. Sci. **40**, 1344–1354 (2009). https://doi.org/10.1007/s11661-009-9830-4
26. S. M. Al-Jaff, Investigation the effective atomic number, electron density, Half value layer and mean free path of steel types 304 and 347 in the energy range 40–130 KeV. J. Nat. Sci. Res. **5** (2013). ISSN 2225–0921. https://www.iiste.org/Journals/index.php/JNSR/article/view/9723
27. R. Singh, S. Singh, G. Singh, K. Singh, Gamma radiation shielding properties of steel and iron slags. Sci. Res. (2017). https://doi.org/10.4236/njgc.2017.71001
28. H. Hosono, Layered iron pnictide superconductors: discovery and current status. J. Phys. Soc. Jpn. **77**, 1–8 (2008). https://doi.org/10.1143/JPSJS.77SC.1
29. R.M. Hamad, T.S. Kayed, S. Kunwar, K.A. Elsayed, E. Abu-Ruz, K.A. Ziq, Effects of iron contents on the vortex state in $Fe_xSe_{0.5}Te_{0.5}$. J. Superconductivity Novel Magnet. **31**(6), 1727–1732 (2018). https://doi.org/10.1007/s10948-017-4391-z
30. M.I. Sayyed, K.A. Mahmoud, E. Lacomme, M.M. AlShammari, N. Dwaikat, Y.S.M. Alajerami, M. Alqahtani, B.O. Elbashir, M.H.A. Mhareb, Development of a novel MoO_3-doped borate glass network for gamma-ray shielding applications. Eur. Phys. J. **136**(1), 1–16 (2021). https://doi.org/10.1140/epjp/s13360-020-01011-5
31. M. Hamad, Bragg-curve simulation of carbon-ion beams for particle-therapy applications: a study with the GEANT4 toolkit. Nuclear Eng. Technol. **53**, 2767–2773 (2021). https://doi.org/10.1016/j.net.2021.02.011
32. Kolmogorov-Smirnov Test, *In: The Concise Encyclopedia of Statistics* (Springer, New York, 2008). https://doi.org/10.1007/978-0-387-32833-1_214
33. K.M. Kaky, M.I. Sayyed, M.H.A. Mhareb, A.H. Abdalsalam, K.A. Mahmoud, S.O. Baki, M.A. Mahdi, Physical, structural, optical and gamma radiation attenuation properties of germanate-tellurite glasses for shielding applications. J. Non Cryst. Solids **545**, 120250 (2020). https://doi.org/10.1016/j.jnoncrysol.2020.120250
34. M.H.A. Mhareb, M. Zeama, M. Elsafi et al., Radiation shielding features for various tellurium-based alloys: a comparative study. J. Mater. Sci. Mater. Electron. (2021). https://doi.org/10.1007/s10854-021-07057-0

Publisher's Note Springer Nature remains neutral with regard to jurisdictional claims in published maps and institutional affiliations.